ISSN 1063-7761, Journal of Experimental and Theoretical Physics, 2007, Vol. 104, No. 3, pp. 436–444. © Pleiades Publishing, Inc., 2007.
Original Russian Text © S.G. Ovchinnikov, Yu.S. Orlov, 2007, published in Zhurnal Éksperimental'noĭ i Teoreticheskoĭ Fiziki, 2007, Vol. 131, No. 3, pp. 485–493.

ORDER, DISORDER, AND PHASE TRANSITIONS IN CONDENSED SYSTEMS

Covalence-Induced Stabilization of an Intermediate-Spin State and the Magnetic Susceptibility of $LaCoO_3$

S. G. Ovchinnikov[a], * and Yu. S. Orlov[b]

[a] *Kirenskiĭ Institute of Physics, Siberian Division, Russian Academy of Sciences, Akademgorodok, Krasnoyarsk, 660036 Russia*

[b] *Krasnoyarsk State University, Krasnoyarsk, 660041 Russia*

**e-mail: sgo@iph.krasn.ru*

Received July 3, 2006

Abstract—The energies of terms with spins $S = 0, 1, 2$ have been found using exact diagonalization of the multielectron Hamiltonian of a multiband *pd* model for the CoO_6 cluster. Co (e_g orbital)–O hops, which form the covalent σ bond, are shown to decrease the energy of the state (IS) with an intermediate spin ($S = 1$) as compared to the energy of the state (LS) with a low spin ($S = 0$). An analogue of the Tanabe–Sugano diagram that takes into account the covalence of the CoO_6 cluster is constructed. The state with $S = 1$ is shown to be a ground state at certain model parameters. An increase in temperature is established to decrease the crystal field and, thus, favors the transition of the ground state from LS to IS at $T = 100$ K and the transition of the IS ground state to a state (HS) with a high spin ($S = 2$) at $T = 550$ K. The magnetic susceptibility of $LaCoO_3$ is calculated with allowance for the LS, IS, and HS states and for the fact that the HS state exhibits threefold orbital degeneracy of the t_{2g} shell, which results in an effective orbital moment $L = 1$ and the importance of spin–orbit interaction. The behavior of this magnetic susceptibility agrees well with the experimental $\chi(T)$ dependence of $LaCoO_3$.

PACS numbers: 71.70.Ch, 74.25.Ha, 75.30.Wx

DOI: 10.1134/S1063776107030090

1. INTRODUCTION

The appearance of high-quality single crystals of cobaltites $RCoO_3$ (R is a rare-earth ion) and $RBaCo_2O_{5+y}$ ($0 \le y \le 1$) has revived interest in these materials, which were studied earlier in the form of polycrystals [1, 2]. Two magnetic specific features (near 100 and 500 K) in the susceptibility $\chi(T)$ of $LaCoO_3$ are well known [1, 3, 8]. The ground state of $LaCoO_3$ is a nonmagnetic dielectric with a low-spin (LS, $S = 0$) state of Co^{3+} with the configuration t_{2g}^6 in the crystal field of the CoO_6 octahedron. A transition into a paramagnetic state takes place in the vicinity of $T = 100$ K, which is indicated by a sharp increase in $\chi(T)$. However, the spin state of Co^{3+} above $T = 100$ K has been unknown for a long time. According to the Tanabe–Sugano diagram for the d^6 ion (Fig. 1), the crossover between the LS and HS terms is possible as the crystal field $10Dq$ changes [4]. However, experiments indicate that an IS state is more probable. To explain both specific features, the authors of [5] proposed a two-stage model, according to which the transition at $T = 100$ K is related to the thermal excitation of the Co^{3+} ion from the LS to the IS state and a crossover from the IS to the HS state occurs at $T = 500$ K. A decrease in the volume induced by an applied hydrostatic pressure [6, 7] or by a chemical pressure upon the replacement of the La^{3+} ion by another R^{3+} ion of a smaller ionic radius [8, 9] shifts both spin crossovers toward high temperatures and makes them closer to each other. In terms of the two-stage model, this behavior means a decrease in the stability of the IS state. In

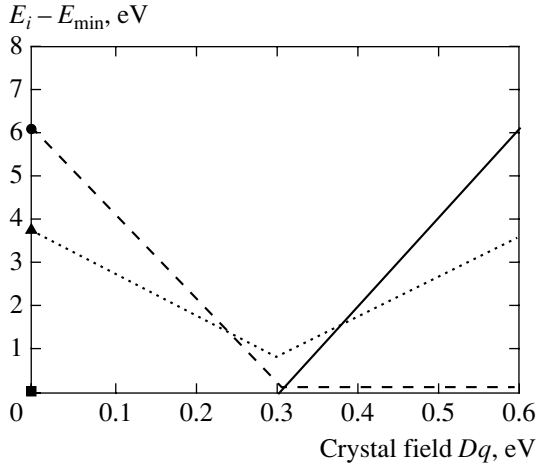

Fig. 1. Tanabe–Sugano diagram for the cobalt ion in a cubic crystal field. The solid line marked by a square stands for the HS state; the dotted line with a triangle, for the IS state; and dashed line with a circle, for the LS state. The calculations were carried out at $U_d = 4$ eV and $V_d = 2.48$ eV.

the framework of the standard model of a d^6 ion in a crystal field [4], the energy of the IS state is so much higher than the LS- and HS-state energies that any thermal filling is impossible (see Fig. 1). It should also be noted that the resistivity decreases significantly above $T = 500$ K, which is related to a smooth dielectric–metal transition [10].

The problem of the IS-state stability has been extensively discussed in the literature [6, 9, 11–14]. Since the IS-state configuration is $t_{2g}^5 e_g^1$, researchers hypothesized that the IS term can be stabilized with respect to the LS state due to covalence. Indeed, the $pd\sigma$ coupling of the cobalt e_g electron with the oxygen p electrons is stronger than the $pd\pi$ coupling characteristic of the t_{2g}^6 configuration of the LS state. This hypothesis was supposed to be supported by first-principles LDA + U calculations with allowance for correlation effects [15]. However, the LDA + U calculations imply spin splitting of the electronic-state energies, which can be justified in magnetically ordered substances. Since $LaCoO_3$ has no long-range order, it is unlikely that the proof of the stabilization of the IS state based on the LDA + U calculations is grounded. A similar problem of the stability of the IS state of the Co^{3+} ion in CoO_5 pyramidal complexes has recently been considered in [16] in terms of a theory of crystal field with effective ion charges, which indirectly reflects covalence effects. The calculations of [16] demonstrate the IS state can be stabilized in $RBaCo_2O_{5+y}$. Nevertheless, covalence effects with the construction of Co–O orbitals and the effects of strong electron correlations forming d^n terms with various spin and orbital moments have not yet been taken into account.

To do this, we perform exact diagonalization of the Hamiltonian of a multiband pd model for the CoO_6 cluster. As a result, we find exact multielectron molecular orbitals, each of which is numbered by the total number of Co (n_d) and oxygen (n_p) electrons (i.e., $n_d + n_p$), the spin, and the orbital moment. Neglecting covalence, we speak about the d^6p^6 configuration having $S = 0, 1, 2$. Covalence results in mixing the configurations $d^6p^6 + d^7p^5$, etc., which are involved in multielectron molecular orbitals. Each of these orbitals is characterized by a certain spin S. By comparing the energies of the LS, IS, and HS states of multielectron molecular orbitals, we could reveal a series of LS $\longrightarrow$ IS and IS $\longrightarrow$ HS crossovers and find a region of the initial-Hamiltonian parameters in which the IS state is a ground state.

In the second part of the work, we calculate the magnetic susceptibility $\chi(T)$ with a model that assumes that the energies of the LS, IS, and HS terms are close to the energy of the ground LS state, which corresponds to $LaCoO_3$. The calculated $\chi(T)$ temperature dependence agrees well with experimental data.

2. EXACT DIAGONALIZATION OF THE CoO_6 CLUSTER

$LaCoO_3$ is a dielectric with a perovskite structure having orthorhombic distortions. Although the CoO_6 cluster in our calculations is considered as an undistorted octahedron, even this approximation can be used to correctly understand the physics of the phenomenon. Small uniaxial contributions to the crystal field can only shift the LS-state stability boundaries.

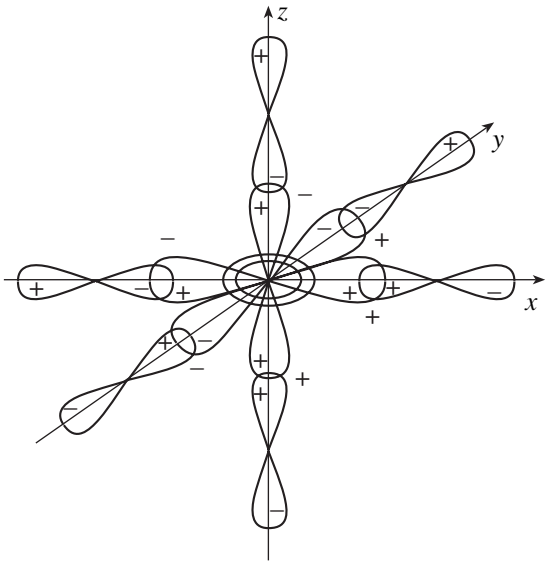

Fig. 2. Atomic orbitals of the cobalt–oxygen cluster involved in the $pd\sigma$ bond.

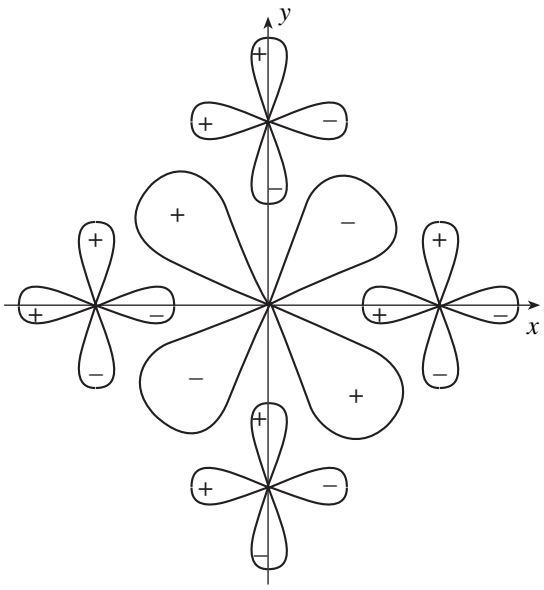

Fig. 3. Atomic orbitals of the cobalt–oxygen cluster involved in the $pd\pi$ bond and shown for the xy plane (the picture for the yz and zx planes is analogous).

The wavefunctions and the signs of hopping integrals for the CoO_6 cluster are shown in Figs. 2 and 3.

We write the Hamiltonian of the oxygen $2p$ and cobalt $3d$ electrons using hole representation for oxygen and electron representation for cobalt:

$$H_{\text{tot}} = H^{(d)} + H^{(p)} + H^{(pd)} + H^{(pp)}, \quad (1)$$

where

$$H^{(d)} = \sum_{\lambda\sigma}\left[(\varepsilon_{d\lambda} - \mu)d^{+}_{\lambda\sigma}d_{\lambda\sigma} + \frac{1}{2}U_d n^{\sigma}_{\lambda} n^{-\sigma}_{\lambda}\right]$$

$$+ \sum_{\substack{\sigma,\sigma' \\ \lambda>\lambda'}}\left(V_d - \frac{J_d}{2}\right)n^{\sigma}_{\lambda}n^{\sigma'}_{\lambda'} - 2J_d\sum_{\lambda>\lambda'}\mathbf{S}_{\lambda}\mathbf{S}_{\lambda'},$$

$$H^{(p)} = \sum_{i}\sum_{\alpha\sigma}\left[-(\varepsilon_{p\alpha} - \mu)p^{+}_{i\alpha\sigma}p_{i\alpha\sigma} + \frac{1}{2}U_p n^{\sigma}_{i\alpha}n^{-\sigma}_{i\alpha}\right]$$

$$+ \sum_{\substack{\sigma,\sigma' \\ \alpha>\alpha'}}\left(V_p - \frac{J_p}{2}\right)n^{\sigma}_{i\alpha}n^{\sigma'}_{i\alpha'} - 2J_p\sum_{\alpha>\alpha'}\mathbf{S}_{i\alpha}\mathbf{S}_{i\alpha'},$$

$$H^{(pd)} = \sum_{i}\sum_{\alpha\lambda\sigma\sigma'}(t_{\lambda\alpha}(d^{+}_{\lambda\sigma}p^{+}_{i\alpha\sigma} + \text{H.c.}) - V_{\lambda\alpha}n^{\sigma}_{\lambda}n^{\sigma'}_{i\alpha}),$$

$$H^{(pp)} = \sum_{i,j}\sum_{\alpha\beta\sigma}(-t_{\alpha\beta}p^{+}_{i\alpha\sigma}p_{j\beta\sigma} + \text{H.c.}).$$

For convenience and clarity, we rewrite this Hamiltonian using oxygen molecular orbitals, which are linear combinations of the wavefunctions of oxygen atoms

$$b_z = \frac{1}{\sqrt{2}}\left(-p_z\left(z+\frac{1}{2}\right) + p_z\left(z-\frac{1}{2}\right)\right),$$

$$b = \frac{1}{2}\left(-p_x\left(x-\frac{1}{2}\right) + p_y\left(y+\frac{1}{2}\right)\right.$$

$$\left. + p_x\left(x+\frac{1}{2}\right) - p_y\left(y-\frac{1}{2}\right)\right),$$

$$a = \frac{1}{2}\left(p_x\left(x-\frac{1}{2}\right) + p_y\left(y+\frac{1}{2}\right)\right.$$

$$\left. - p_x\left(x+\frac{1}{2}\right) - p_y\left(y-\frac{1}{2}\right)\right).$$

We also use b_μ, where $\mu = xy, yz, zx$; that is,

$$b_{xy} = \frac{1}{2}\left(p_y\left(x-\frac{1}{2}\right) + p_x\left(y+\frac{1}{2}\right)\right.$$

$$\left. - p_y\left(x+\frac{1}{2}\right) - p_x\left(y-\frac{1}{2}\right)\right),$$

and b_{yz} and b_{zx} are obtained from b_{xy} via cyclic permutation of the subscripts xyz. Moreover, we use a_μ, where $\mu = xy, yz, zx$; that is,

$$a_{xy} = \frac{1}{2}\left(p_y\left(x-\frac{1}{2}\right) - p_x\left(y+\frac{1}{2}\right)\right.$$

$$\left. - p_y\left(x+\frac{1}{2}\right) + p_x\left(y-\frac{1}{2}\right)\right),$$

and a_{yz} and a_{zx} are obtained from a_{xy} via cyclic permutation of the subscripts xyz. Any next permutation in a_μ should be accompanied by a change in the sign of each term entering into a linear combination.

In this basis, Hamiltonian (1) takes the form

$$H_{\text{tot}} = H^{(d)} + H^{(p)} + H^{(pd)}_{\text{Coulomb}} + H^{(pd)}_{\text{hop}} + H^{(pp)}_{\text{hop}}, \quad (2)$$

$$H^{(d)} = \sum_{\lambda,\sigma}\left(\varepsilon_{d_\lambda}d^{+}_{\lambda,\sigma}d_{\lambda,\sigma} + \frac{1}{2}U_d n_{\lambda\sigma}n_{\lambda\bar{\sigma}}\right)$$

$$+ \sum_{\substack{\sigma,\sigma' \\ \lambda>\lambda'}}\left(V_d - \frac{J_d}{2}\right)n^{\sigma}_{\lambda}n^{\sigma'}_{\lambda'} - 2J_d\sum_{\lambda>\lambda'}\mathbf{S}_{\lambda}\mathbf{S}_{\lambda'},$$

$$H^{(p)} = \sum_{\mu,\sigma}-\varepsilon_{b_\mu}b^{+}_{\mu,\sigma}b_{\mu,\sigma} + \sum_{\sigma}-\varepsilon_b b^{+}_{\sigma}b_{\sigma}$$

$$+ \sum_{\sigma}-\varepsilon_a a^{+}_{\sigma}a_{\sigma} + \sum_{\sigma}-\varepsilon_{b_z}b^{+}_{z,\sigma}b_{z,\sigma}$$

$$+ \sum_{\xi,\sigma}\left(\frac{1}{2}U_p n_{\xi\sigma}n_{\xi\bar{\sigma}}\right) + \sum_{\xi>\xi'}\left(V_p - \frac{J_p}{2}\right)n^{\sigma}_{\xi}n^{\sigma'}_{\xi'}$$

$$- 2J_p\sum_{\xi>\xi'}\mathbf{S}_{\xi}\mathbf{S}_{\xi'},$$

$$H^{(pd)}_{\text{Coulomb}} = \sum_{\substack{\sigma,\sigma' \\ \lambda,\xi}}(-V_{pd})n^{\sigma}_{\lambda}n^{\sigma'}_{\xi},$$

$$H_{\text{hop}}^{(pd)} = \sum_{\mu} H_{\mu}^{(pd)} + H_{d_x}^{(pd)} + H_{d_z}^{(pd)},$$

$$H_{\mu}^{(pd)} = 2\sum_{\sigma} t_{pd}^{\pi}(d_{\mu,\sigma}^{+} b_{\mu,\bar{\sigma}}^{+} + \text{H.c.}),$$

$$H_{d_x}^{(pd)} = 2\sum_{\sigma} t_{pd}^{\sigma}(d_{x,\sigma}^{+} b_{\bar{\sigma}}^{+} + \text{H.c.}),$$

$$H_{d_z}^{(pd)} = 2\sum_{\sigma} \frac{t_{pd}^{\sigma}}{\sqrt{3}}(d_{z,\sigma}^{+} a_{\bar{\sigma}}^{+} + \text{H.c.})$$

$$+ \sqrt{2}\sum_{\sigma} t_{pd}^{'\sigma}(d_{z,\sigma}^{+} b_{z,\bar{\sigma}}^{+} + \text{H.c.}),$$

$$H_{\text{hop}}^{(pp)} = \sum_{\mu} H_{\mu}^{(pp)} + H_{xyz}^{(pp)},$$

$$H_{\mu}^{(pp)} = -2\sum_{\sigma} t_{pp}^{\pi} b_{\mu,\sigma}^{+} b_{\mu,\sigma} + 2\sum_{\sigma} t_{pp}^{\pi} a_{\mu,\sigma}^{+} a_{\mu,\sigma}$$

$$-\frac{1}{3}\left\{2\sum_{\sigma} t_{pp}^{\pi} a_{\sigma}^{+} a_{\sigma} - 2\sum_{\sigma} t_{pp}^{\pi} b_{\sigma}^{+} b_{\sigma}\right\},$$

$$H_{xyz}^{(pp)} = 2\sqrt{2}\sum_{\sigma} t_{pp}^{\pi}(a_{\sigma}^{+} b_{z,\sigma} + \text{H.c.}).$$

Here, the first two terms describe the energies of cobalt d electrons and oxygen p holes with allowance for the following Coulomb interactions: Hubbard repulsion U_d (U_p), orbit–orbit intraatomic and intramolecular Coulomb repulsion V_d (V_p), and Hund exchange interaction J_d (J_p). The subscripts λ and ξ correspond to different cobalt atomic orbitals and oxygen molecular orbitals: $\lambda = (t, e)$, where $t = xy, yz, zx$; $e = x^2 - y^2, 3z^2 - r^2$; and $\xi = b, a, b_z, b_\mu, a_\mu$. The third and fourth terms describe pd hops and hole–electron Coulomb interaction V_{pd}. The last term corresponds to pp hops.

In electrically neutral $La^{3+}Co^{3+}O_3^{2-}$, the cobalt ion can occupy three different spin states, namely, HS ($t_{2g}^4 e_g^2$, $S = 2$), IS ($t_{2g}^5 e_g^1$, $S = 1$), and LS ($t_{2g}^6 e_g^0$, $S = 0$) states (Fig. 4). The formation of each state depends on the balance between the crystal-field splitting energy Δ and the intraatomic exchange interaction energy J. The

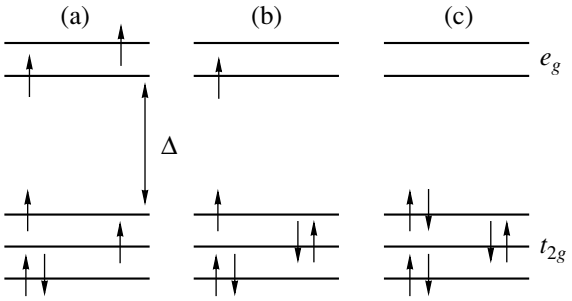

Fig. 4. States with a (a) high, (b) intermediate, or (c) low spin.

initial ionic configuration is $d^6 p_N^6$ (six electrons on cobalt and six electrons on each of the six ($N = 6$) oxygen atoms). However, electron jumps accompanied by hole formation on molecular orbitals and electron production on the cobalt site are possible due to the overlapping of the wavefunctions $d_{x^2-y^2} \equiv d_x$, $d_{3z^2-r^2} \equiv d_z$, d_{xy}, d_{zy}, and d_{xz} with the oxygen molecular orbitals and to the presence of free positions not forbidden by the Pauli exclusion principle. Therefore, apart from the initial $d^6 p_6^6$ configuration, $d^7 p^5 p_5^6$, $d^8 p_2^5 p_4^6$, $d^8 p^4 p_5^6$, etc., electronic configurations can also appear. Each of the three spin states has its specific set of vectors, which represent various combinations of hole and electron distributions over one-to-one states. They can be written explicitly using second quantization.

For example, in the case of the HS state for the $d^6 p_6^6$ configuration, we have the set

$$e_{1\sigma}^{+} e_{2\sigma}^{+} t_{1\sigma}^{+} t_{2\sigma}^{+} t_{3\sigma}^{+} t_{j\bar{\sigma}}^{+} |\text{vac}\rangle, \quad j = 1, 2, 3,$$

where $|\text{vac}\rangle = |d^0 p^6 L_a^{3+}\rangle$. For the $d^7 p^5 p_5^6$ configuration at $j = 1$, we have several versions of the location of an additional d electron and an oxygen hole:

1) $e_{1\uparrow}^{+} e_{2\uparrow}^{+} t_{1\uparrow}^{+} t_{2\uparrow}^{+} t_{3\uparrow}^{+} t_{1\downarrow}^{+} b_{yz\uparrow}^{+} |\text{vac}\rangle = |\text{HS}, d^7 p^5 p_5^6(1)\rangle$,

2) $-e_{1\uparrow}^{+} e_{2\uparrow}^{+} t_{1\uparrow}^{+} t_{2\uparrow}^{+} t_{3\uparrow}^{+} t_{3\downarrow}^{+} t_{1\downarrow}^{+} b_{zx\uparrow}^{+} |\text{vac}\rangle = |\text{HS}, d^7 p^5 p_5^6(2)\rangle$,

3) $-e_{1\uparrow}^{+} e_{1\downarrow}^{+} e_{2\uparrow}^{+} t_{1\uparrow}^{+} t_{2\uparrow}^{+} t_{3\uparrow}^{+} t_{1\downarrow}^{+} b_{\uparrow}^{+} |\text{vac}\rangle = |\text{HS}, d^7 p^5 p_5^6(3)\rangle$,

4) $e_{1\uparrow}^{+} e_{2\uparrow}^{+} e_{2\downarrow}^{+} t_{1\uparrow}^{+} t_{2\uparrow}^{+} t_{3\uparrow}^{+} t_{1\downarrow}^{+} a_{\uparrow}^{+} |\text{vac}\rangle = |\text{HS}, d^7 p^5 p_5^6(4)\rangle$,

5) $e_{1\uparrow}^{+} e_{2\uparrow}^{+} e_{2\downarrow}^{+} t_{1\uparrow}^{+} t_{2\uparrow}^{+} t_{3\uparrow}^{+} t_{1\downarrow}^{+} b_{z\uparrow}^{+} |\text{vac}\rangle = |\text{HS}, d^7 p^5 p_5^6(5)\rangle$.

In the case of the LS state for the $d^6 p_6^6$ configuration, we have the ground state (Fig. 4c)

$$|0\rangle = t_{1\uparrow}^{+} t_{1\downarrow}^{+} t_{2\uparrow}^{+} t_{2\downarrow}^{+} t_{3\uparrow}^{+} t_{3\downarrow}^{+} |\text{vac}\rangle,$$

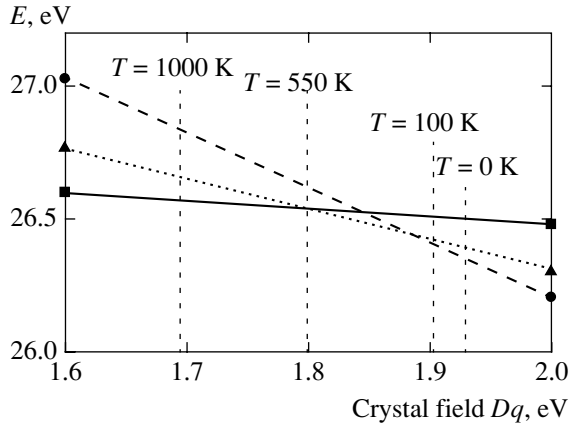

Fig. 5. Analogue of the Tanabe–Sugano diagram for the multielectron molecular orbitals of the CoO_6 cluster. The designations are identical to those in Fig. 1. The calculations were carried out at $\beta = 0.4$, $t_{pp}^{\pi} = 0.2$ eV, $t_{pd}^{\sigma} = 1.85$ eV, $\varepsilon_p = 1.5$ eV, $U_d = 4$ eV and $V_d = 2.48$ eV, and $V_{pd} = 1.8$ eV.

and, for the $d^7p^5p_5^6$ configuration, we find

$$1)\ e_{1\uparrow}^{+}b_{\downarrow}^{+}|0\rangle = |\mathrm{LS}, d^7p^5p_5^6(1)\rangle,$$
$$2)\ e_{1\downarrow}^{+}b_{\uparrow}^{+}|0\rangle = |\mathrm{LS}, d^7p^5p_5^6(2)\rangle,$$
$$3)\ e_{2\uparrow}^{+}a_{\downarrow}^{+}|0\rangle = |\mathrm{LS}, d^7p^5p_5^6(3)\rangle,$$
$$4)\ e_{2\downarrow}^{+}a_{\uparrow}^{+}|0\rangle = |\mathrm{LS}, d^7p^5p_5^6(4)\rangle,$$
$$5)\ e_{2\uparrow}^{+}b_{z\downarrow}^{+}|0\rangle = |\mathrm{LS}, d^7p^5p_5^6(5)\rangle,$$
$$7)\ e_{2\downarrow}^{+}b_{z\uparrow}^{+}|0\rangle = |\mathrm{LS}, d^7p^5p_5^6(6)\rangle.$$

For the $d^6p_6^6$ IS state, we have the following six terms (Fig. 4b):

$$e_{i\sigma}^{+}t_{j\bar{\sigma}}|0\rangle, \quad i = 1, 2, \quad j = 1, 2, 3.$$

For the $d^7p^5p_5^6$ IS state, the following terms are generated:

$$1)\ -e_{2\uparrow}^{+}b_{xy\uparrow}^{+}|0\rangle = |\mathrm{IS}, d^7p^5p_5^6(1)\rangle,$$
$$2)\ e_{1\uparrow}^{+}e_{2\uparrow}^{+}t_{1\downarrow}b_{\downarrow}^{+}|0\rangle = |\mathrm{IS}, d^7p^5p_5^6(2)\rangle,$$
$$3)\ e_{1\downarrow}^{+}e_{2\uparrow}^{+}t_{1\downarrow}b_{\uparrow}^{+}|0\rangle = |\mathrm{IS}, d^7p^5p_5^6(3)\rangle,$$
$$\text{for } i = 2, \quad j = 1,$$
$$4)\ -e_{2\uparrow}^{+}e_{2\downarrow}^{+}t_{1\downarrow}a_{\uparrow}^{+}|0\rangle = |\mathrm{IS}, d^7p^5p_5^6(4)\rangle,$$
$$5)\ -e_{2\uparrow}^{+}e_{2\downarrow}^{+}t_{1\downarrow}b_{z\uparrow}^{+}|0\rangle = |\mathrm{IS}, d^7p^5p_5^6(5)\rangle,$$

or

$$\begin{cases} -e_{1\uparrow}^{+}b_{xy\uparrow}^{+}|0\rangle, \\ e_{1\downarrow}^{+}e_{1\uparrow}^{+}t_{1\downarrow}b_{\uparrow}^{+}|0\rangle, \\ -e_{1\uparrow}^{+}e_{2\uparrow}^{+}t_{1\downarrow}a_{\downarrow}^{+}|0\rangle, \\ -e_{1\uparrow}^{+}e_{2\downarrow}^{+}t_{1\downarrow}a_{\uparrow}^{+}|0\rangle, \\ -e_{1\uparrow}^{+}e_{2\uparrow}^{+}t_{1\downarrow}b_{z\downarrow}^{+}|0\rangle, \\ -e_{1\uparrow}^{+}e_{2\downarrow}^{+}t_{1\downarrow}b_{z\uparrow}^{+}|0\rangle \end{cases} \quad \text{for } i = 1, \quad j = 1.$$

Generally speaking, the next *pd* jump can transform the $d^7p^5p_5^6$ configuration into the $d^8p_2^5p_4^6$ and, then, the $d^9p_3^5p_3^6$ configuration; however, the probability of such configurations is extremely small, and they may be neglected.

The diagonalization of the matrices of Hamiltonian (2), which were obtained for each of the HS, IS, and LS states and were written in their specific bases (the matrix block for the HS state is given in the Appendix, and the matrices of the IS and LS states are similar) can be used to construct an analogue of the Tanabe–Sugano diagram that takes into account the covalence of the CoO_6 cluster (Fig. 5). Figure 5 shows the lowest eigenvalues, since they are of particular interest for the physics of low energies.

We find that, in a certain region of the parameters U_d, V_d, J_d, V_{pd}, Δ, t_{pp}^{π}, t_{pd}^{σ}, ε_p, and β (where $\beta = t_{pd}^{\prime\sigma}/t_{pd}^{\sigma}$), the intermediate state can be stabilized due to the hybridization of the Co e_g level and the O $2p$ level.

3. TEMPERATURE AND PRESSURE DEPENDENCES OF THE CRYSTAL FIELD

$LaCoO_3$ is known to exhibit anomalously large compressibility of the Co–O bond length L, $\beta_L = -L^{-1}(\partial L/\partial P)_T = 4.8 \times 10^{-3}$ GPa^{-1} [17]. This is the maximal B–O bond compressibility among all the ABO_3 perovskites. This large compressibility is likely to lead to a rather strong temperature dependence of the bond length. For example, $L = 1.9345$ Å at $T = 300$ K and $L = 1.9254$ Å at $T = 5$ K [18]. It can easily be estimated that a decrease in the temperature from 300 to 5 K is equivalent to an applied pressure of $\delta P = \delta L/L\beta_L \approx 1$ GPa. Whence, it follows that the crystal field $\Delta = 10Dq$ also decreases noticeably with increasing temperature, since Δ increases with pressure. To estimate this dependence, we use the first-principles calculation of Δ for $LaCoO_3$ ($\Delta = 1.93$ eV) and for $HoCoO_3$ ($\Delta = 2.04$ eV) [19]. The increase in Δ upon the replacement of the La^{3+} ion by

the smaller Ho^{3+} ion is caused by chemical compression. In $HoCoO_3$ at $T = 300$ K, the Co–O bond length $L = 1.921$ Å [19]. Thus, we can write

$$\Delta(T) = \Delta(0) + \frac{\partial\Delta}{\partial L}\frac{\partial L}{\partial T}T$$

and can estimate $\partial\Delta/\partial L$ from the chemical compression caused by substitution of Ho for La. As a result, we obtain $\partial\Delta/\partial L \approx -8$ eV/Å. Finally, for $LaCoO_3$ we find $\Delta(T) \approx \Delta(0) - 0.24 \times 10^{-3}T$. In Fig. 5, the crystal fields corresponding to the temperatures that are most important for the behavior of the magnetic susceptibility are indicated. A decrease in the crystal field with increasing temperature favors the filling of the intermediate- and high-spin terms from the ground low-spin term (Fig. 5).

The pressure dependence of the crystal field can also be estimated as

$$\Delta(P) = \Delta(0) + \alpha_\Delta P,$$
$$\alpha_\Delta = \frac{\partial\Delta}{\partial L}\frac{\partial L}{\partial P} = -\beta_L\frac{\partial\Delta}{\partial L}L.$$

Using the estimates of the Co–O bond compressibility and the derivative $\partial\Delta/\partial L$ given above, we find $\alpha_\Delta = 0.0726$ eV/GPa. Note that this value is more than three times that of $FeBO_3$ ($\alpha_\Delta = 0.020$ eV/GPa [20]).

4. MAGNETIC SUSCEPTIBILITY

An analytical expression for the magnetic susceptibility can be obtained from the consideration of a three-level system in a magnetic field. We have to take into account that the HS state has threefold orbital degeneracy of the t_{2g} shell, which results in an effective orbital moment $L = 1$ and the importance of spin–orbit interaction. We now consider a certain lattice site and introduce the following designations:

$$E_{LS} = E_0,$$
$$E_{IS} = E_1 - g_{IS}\mu\mathbf{B}\cdot\mathbf{S} = E_1 - g_{IS}\mu m_S B,$$
$$m_S = S, S-1, \ldots, -S, \quad S = 1,$$
$$E_{HS} = E_2 - g_{HS}\mu\mathbf{B}\cdot\mathbf{J} = E_2 - g_{HS}\mu m_{\tilde{J}} B,$$
$$m_{\tilde{J}} = \tilde{J}, \tilde{J}-1, \ldots, -\tilde{J}, \quad \tilde{J} = 1.$$

Here, E_i ($i = 0, 1, 2$) is the term energy in the absence of a magnetic field; μ is the Bohr magneton; $g_{IS} = 2$ and $g_{HS} = 2.5$ are the Landé splitting factors of the IS and HS states, respectively; $\tilde{J}$ is the total effective moment for the HS state, which is equal to unity because of spin–orbit interaction and more than half-filled $3d$ subshell of the cobalt atom [21]; and $\mathbf{B}$ is the applied magnetic field.

Since $LaCoO_3$ is a dielectric, intercluster hops are insignificant, and the system can be considered as a set of noninteracting (to a first approximation) unit cells with one CoO_6 cluster in each of them. Then, the partition function takes the form

$$Z = \exp\left(-\frac{E_{LS}}{kT}\right) + \sum_{m_S=-1}^{1}\exp\left(-\frac{E_{IS}}{kT}\right)$$
$$+ \sum_{m_{\tilde{J}}=-1}^{1}\exp\left(-\frac{E_{HS}}{kT}\right) = \exp\left(-\frac{E_0}{kT}\right)$$
$$\times\left\{1 + \exp\left(-\frac{\Delta_1}{kT}\right)\sum_{m_S=-1}^{1}\exp\left(\frac{g_{IS}\mu m_S B}{kT}\right)\right.$$
$$\left. + \exp\left(-\frac{\Delta_2}{kT}\right)\sum_{m_{\tilde{J}}=-1}^{1}\exp\left(\frac{g_{HS}\mu m_{\tilde{J}} B}{kT}\right)\right\},$$

where $\Delta_1 = E_1 - E_0$, $\Delta_2 = E_2 - E_0$, and k is the Boltzmann constant. Since the crystal field Δ is a function of temperature, the quantities Δ_1 and Δ_2 are also temperature-dependent:

$$\Delta_1(T) = \Delta_1(0) - (K_1 - K_0)\frac{\partial\Delta}{\partial L}\frac{\partial L}{\partial T}T$$
$$= \Delta_1(0) - (K_1 - K_0)\times 0.24\times 10^{-3}T,$$
$$\Delta_2(T) = \Delta_2(0) - (K_2 - K_0)\frac{\partial\Delta}{\partial L}\frac{\partial L}{\partial T}T$$
$$= \Delta_2(0) - (K_2 - K_0)\times 0.24\times 10^{-3}T,$$

where K_0, K_1, and K_2 are the slopes of the terms $E_0 = E_0(\Delta)$, $E_1 = E_1(\Delta)$, and $E_2 = E_2(\Delta)$ to the crystal-field axis (see Fig. 5). Finally, we obtain

$$\Delta_1(T) \approx \Delta_1(0) - 0.24\times 10^{-3}T,$$
$$\Delta_2(T) \approx \Delta_2(0) - 0.43\times 10^{-3}T.$$

At $T \approx 8$ K, $\Delta_1(T)$ is known to vary from 0.012 to 0.025 eV [5, 6, 22–24]. Therefore, $\Delta_1(0)$ is taken to be 0.025 eV, which agrees satisfactorily with the exact diagonalization calculations performed earlier (see

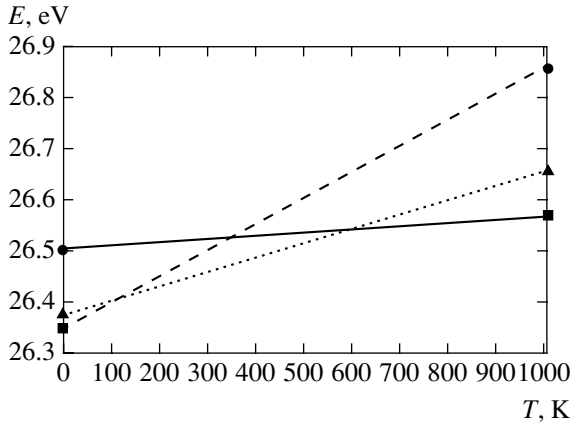

Fig. 6. Temperature dependences of the term energy. The designations are identical to those in Fig. 1.

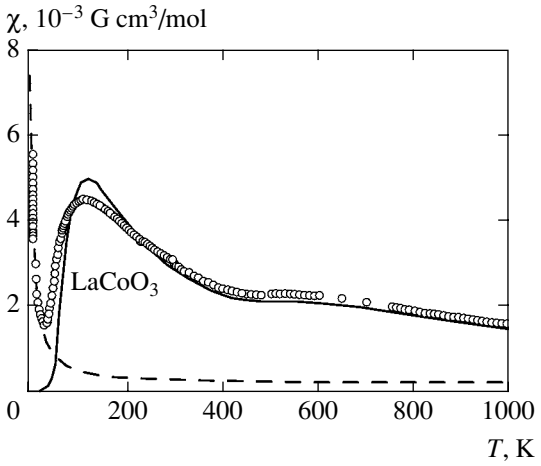

Fig. 7. Magnetic susceptibility of $LaCoO_3$ calculated at $\Delta_1(0) = 0.025$ eV and $\Delta_2(0) = 0.15$ eV: (solid line) our calculation, (circles) experimental points, and (dashed line) extrapolation of the contribution of paramagnetic impurities [8].

Fig. 5 or 6), and $\Delta_2(0) = 0.15$ eV is a parameter determined from the same calculations.

Given the partition function, we find the free energy $F = -kT\ln Z$ and the magnetization $M = -\Delta F/\Delta B$ by a standard procedure.

For moderate temperatures and magnetic fields, at $g_{HS(LS)}\mu B \ll kT$, we obtain the following expression for the magnetic susceptibility of one mole containing N_A unit cells:

$$\chi = \frac{\Delta M}{\Delta B} = N_A \frac{2\mu^2}{kT} \frac{g_{IS}^2 \exp\left(-\frac{\Delta_1}{kT}\right) + g_{HS}^2 \exp\left(-\frac{\Delta_2}{kT}\right)}{1 + 3\exp\left(-\frac{\Delta_1}{kT}\right) + 3\exp\left(-\frac{\Delta_2}{kT}\right)}.$$

This expression is illustrated in Fig. 7, which also shows the experimental behavior of the magnetic susceptibility taken from [8] for comparison. The calculated and experimental curves are seen to be similar. To avoid confusion, note that $\chi(T)$ does not vanish at a certain "critical" temperature, as can be concluded from the consideration of Fig. 7 (this is related to the chosen scale). At low temperatures, the magnetic susceptibility is exponentially small but finite. The paramagnetic impurities present in the sample give the contribution proportional to T^{-1}, which was revealed in [8] and is shown as a dashed line in Fig. 7.

Using the stabilization of the IS state and the decrease in the crystal field with increasing temperature, we can describe the behavior of the magnetic susceptibility of $LaCoO_3$. At $T \approx 0$ K ($\Delta = 1.93$ eV), the Co^{3+} ions are in the ground LS state. As the temperature increases, the population of the higher IS ($\Delta_1(0) = 0.025$ eV) and HS ($\Delta_2(0) = 0.15$ eV) states increases. At $T \approx 100$ K, the crystal field shifts toward low values ($\Delta = 1.9$ eV), and the ground state transforms from the LS to the IS state (see Fig. 6). A further increase in the temperature to $\Delta \approx 550$ K leads to a larger decrease in the crystal field ($\Delta = 1.8$ eV) and to the transformation of the ground state to the HS state. As a result, the specific features of the magnetic susceptibility at 100 and 500 K become clear. In this work, we do not consider the metallization of $LaCoO_3$, since this requires further calculations.

5. CONCLUSIONS

Using exact diagonalization of the multielectron Hamiltonian of a multiband *pd* model for the CoO_6 cluster, we found the states and energies of terms with spins $S = 0, 1, 2$. We revealed the following main causes of the strange behavior of the magnetic susceptibility of $LaCoO_3$: a decrease in the crystal field with increasing temperature; threefold orbital degeneracy of the t_{2g} shell (which results in an effective orbital moment $L = 1$ and the importance of spin–orbit interaction); and the fact that Co (e_g orbital)–O hops, which form the covalent σ bond, decrease the energy of the IS ($S = 1$) state as compared to the LS ($S = 0$) state. We found a parameter region where the state with $S = 1$ is a ground state. The magnetic susceptibility calculated with allowance for the LS, IS, and HS states agrees well with the experimental $\chi(T)$ dependence of $LaCoO_3$. The maximum in $\chi(T)$ at $t = 100$ K is related to the thermal filling of the IS state and its stabilization with increasing T, and the plateau in the range 550–600 K is caused by the contribution of the HS state.

APPENDIX

The matrix block of Hamiltonian (2) written for the HS state.

Table

	$d^6p^6, j=1$	$d^7p^5p_5^6(1)$	$d^7p^5p_5^6(2)$	$d^7p^5p_5^6(3)$	$d^7p^5p_5^6(4)$	$d^7p^5p_5^6(5)$
$d^6p^6, j=1$	$6\varepsilon_d - 4dq + U_d + 14V_d - 10J_d$	$2t_{pd}^{\pi}$	$2t_{pd}^{\pi}$	$2t_{pd}^{\sigma}$	$2\frac{t_{pd}^{\sigma}}{\sqrt{3}}$	$\sqrt{2}t_{pd}^{'\sigma}$
$d^7p^5p_5^6(1)$	$2t_{pd}^{\pi}$	$7\varepsilon_d - 8dq + 2U_d + 19V_d - 11J_d - 7V_{pd} - 2t_{pp} - \varepsilon_p$	–	–	–	–
$d^7p^5p_5^6(2)$	$2t_{pd}^{\pi}$	–	$7\varepsilon_d - 8dq + 2U_d + 19V_d - 11J_d - 7V_{pd} - 2t_{pp} - \varepsilon_p$	–	–	–
$d^7p^5p_5^6(3)$	$2t_{pd}^{\sigma}$	–	–	$7\varepsilon_d + 2dq + 2U_d + 19V_d - 11J_d - 7Vp_d + 2t_{pp} - \varepsilon_p$	–	–
$d^7p^5p_5^6(4)$	$2\frac{t_{pd}^{\sigma}}{\sqrt{3}}$	–	–	–	$7\varepsilon_d + 2dq + 2U_d + 19V_d - 11J_d - 7V_{pd} - 2t_{pp} - \varepsilon_p$	$2\sqrt{2}t_{pp}^{\pi}$
$d^7p^5p_5^6(5)$	$\sqrt{2}t_{pd}^{'\sigma}$	–	–	–	$2\sqrt{2}t_{pp}^{'\pi}$	$7\varepsilon_d + 2dq + 2U_d + 19V_d - 11J_d - 7V_{pd} - \varepsilon_p$

ACKNOWLEDGMENTS

This work was supported by the program of the Division of Physical Sciences of the Russian Academy of Sciences "Strong Electronic Correlations," the integration project SORAN-URORAN (grant no. 74), and the Krasnoyarsk krai Science Foundation.

REFERENCES

1. P. M. Raccah and J. B. Goodenough, Phys. Rev. **155**, 932 (1967).
2. G. Thornton, F. C. Morrison, S. Partington, et al., J. Phys. C: Solid State Phys. **21**, 2871 (1988).
3. R. R. Heikes, R. C. Miller, and R. Mazelsky, Physica (Amsterdam) **30**, 1600 (1964).
4. Y. Tanabe and S. Sugano, J. Phys. Soc. Jpn. **9**, 766 (1954).
5. K. Asai, A. Yoneda, O. Yokokura, et al., J. Phys. Soc. Jpn. **67**, 290 (1998).
6. K. Asai, O. Yokokura, M. Suzuki, et al., J. Phys. Soc. Jpn. **66**, 967 (1997).
7. T. Vogt, J. A. Hriljac, N. C. Hyatt, et al., Phys. Rev. B **67**, 140401 (2003).
8. J. Baier, S. Jodlank, M. Kreiner, et al., Phys. Rev. B **71**, 014443 (2005).
9. I. A. Nekrasov, S. V. Streltsov, M. A. Korotin, and V. I. Anisimov, Phys. Rev. B **68**, 235113 (2003).
10. Y. Tokura, Y. Okimoto, S. Yamaguchi, et al., Phys. Rev. B **58**, R 1699 (1998).
11. R. H. Potze, G. A. Sawatzky, and M. Abbate, Phys. Rev. B **51**, 11 501 (1995).
12. H. Takahashi, F. Munakata, and M. Yamanaka, Phys. Rev. B **57**, 15 211 (1998).
13. M. Zuang, W. Zhang, An Hu, and N. Ming, Phys. Rev. B **57**, 13 655 (1998).
14. Z. Hu, H. Wu, M. W. Hawerkort, et al., Phys. Rev. Lett. **92**, 207402 (2004).
15. M. A. Korotin, S. Yu. Ezhov, I. V. Solovyev, et al., Phys. Rev. B **54**, 5309 (1996).

16. E. S. Zhitlukhina, K. V. Lamonova, S. M. Orel, and Yu. G. Pashkevich, Fiz. Nizk. Temp. **31**, 1266 (2005).

17. T. Vogt, J. A. Hriljac, N. C. Hyatt, and P. Woodward, Phys. Rev. B **67**, 140401 (2003).

18. P. G. Radaelly and S. W. Cheong, Phys. Rev. B **66**, 094408 (2002).

19. X. Liu and C. T. Prewitt, J. Phys. Chem. Solids **52**, 441 (1991).

20. S. G. Ovchinnikov, V. I. Anisimov, I. A. Nekrasov, and Z. V. Pchelkina, Phys. Met. Metallogr. **99**, Suppl. 1, 593 (2005).

21. A. Abragam and B. Bleaney, *Electron Paramagnetic Resonance of Transition Ions* (Clarendon, Oxford, 1970; Mir, Moscow, 1972).

22. Y. Kobayashi, Thant Sin Naing, M. Suzuki, et al., Phys. Rev. B **72**, 174405 (2002).

23. Y. Kobayashi, N. Fujiwara, S. Murata, et al., Phys. Rev. B **62**, 410 (2000).

24. S. Noguchi, S. Kawamata, K. Okuda, et al., Phys. Rev. B **66**, 094404 (2000).

Translated by K. Shakhlevich